Available online at www.sciencedirect.com

SciVerse ScienceDirect

Ceramics International 39 (2013) 7959–7966

CERAMICS INTERNATIONAL

www.elsevier.com/locate/ceramint

Synthesis and properties of core–shell structured $BaCe_{0.9}Y_{0.1}O_{2.95}$: $BaZr_{0.9}Y_{0.1}O_{2.95}$

Ling Wang*, Chao Jin, Lei Dai, Yue-Hua Li, Jing Zhu, Hui-Zhu Zhou, Li-Mei Zhang

College of Chemical Engineering, Hebei United University, Tangshan 063009, China

Received 16 December 2012; received in revised form 16 March 2013; accepted 16 March 2013
Available online 23 March 2013

Abstract

The perovskite proton conductor $BaZr_{0.9}Y_{0.1}O_{2.95}$ (BZY10) shows better chemical stability but lower conductivity than $BaCe_{0.9}Y_{0.1}O_{2.95}$ (BCY10). In this paper we attempted to synthesize BCY10:BZY10 core–shell materials in which BCY10 particles prepared by solid reaction were wrapped by a sol–gel deposited thin layer of BZY10 with ZnO as sintering aid to improve the sinterability of the materials. The effects of the BCY10/BZY10 ratios on the phase purity, microstructure, chemical stability and electrical conductivity of the samples were characterized by XRD, TEM, SEM, TGA and electrochemical impedance spectroscopy. A dense core–shell structure was formed after being sintered at 1300 °C for 10 h. The core–shell samples displayed improved stability against CO_2 and water vapor at high temperature. With BCY10/BZY10 ratio varying from 9:1 to 7:3, the core–shell samples became more stable, and the total conductivities decreased.

Keywords: A. Sol–gel processes; C. Ionic conductivity; D. Perovskites; Core–shell structured $BaCe_{0.9}Y_{0.1}O_{2.95}$: $BaZr_{0.9}Y_{0.1}O_{2.95}$; Impedance spectrum

1. Introduction

Iwahara et al. [1] first discovered proton conducting perovskite-type oxides in 1981. Since then, it is well-known that perovskite oxides based on doped $BaCeO_3$, $SrCeO_3$, $CaZrO_3$ and $BaZrO_3$ demonstrate good proton conduction under hydrogen-containing atmosphere at high temperature. The high temperature proton conductors (HTPCs) have found a great potential for applications, such as gaseous sensors [2], hydrogen pumps [3], fuel cells [4] and steam electrolyzers [5]. Rare-earth metal-doped $BaCeO_3$ and $BaZrO_3$ have been studied the most widely among the HTPCs. Yttrium doped $BaCeO_3$ conductors show the highest conductivity, but rather poor chemical stability and endurance against CO_2 or H_2O. They gradually decompose into $Ba(OH)_2$/$BaCO_3$ and CeO_2 after being exposed to H_2O/CO_2 atmosphere for some time. In contrast, doped $BaZrO_3$ conductors exhibit excellent chemical stability in H_2O or CO_2 atmosphere, but lower conductivity [6]. Meanwhile, they are highly refractory, requiring to be sintered at a very high temperature (ca. 1700 °C) to obtain fully dense ceramics. So many researchers tried some ways to make a compromise between the high conductivity of $BaCeO_3$-based conductors and the good chemical stability of $BaZrO_3$-based conductors, including the physical mixture of $BaCeO_3$ and $BaZrO_3$, $BaCeO_3$–$BaZrO_3$ solid solution [7,8], and $BaZr_{0.9}Y_{0.1}O_{2.95}$:$BaCe_{0.9}Y_{0.1}O_{2.95}$ core–shell structures [9,10]. According to the core–shell concept, Savaniu et al. [9] improved the conductivity and sintering property of BZY10 by coating the BZY10 grains with a thin layer of BCY10 and found that the proton conductors BZY10:BCY10 with a core–shell structure showed higher conductivity than that of BZY10:BCY10 physical mixture or BZY10:BCY10 solid solution with the same composition as the core–shell structure sample. The way of coating one material with another type of material to improve the properties of the former is a popular approach for the preparation of functional nanomaterials with applications in medicine, photocatalysts, optics, magnetics and sensors [11]. Sol–gel routes are often used for the preparation of core–shell structure materials. This method has advantages, including thin coating, high purity, low sintering temperatures and short times for the densification of materials [12,13].

In order to improve the sinterability of materials, the addition of some transition metal oxides into the materials is a common method. ZnO has been previously reported to be

*Corresponding author. Tel./fax: +86 315 2592170.
E-mail address: tswling@126.com (L. Wang).

0272-8842/$ - see front matter © 2013 Published by Elsevier Ltd and Techna Group S.r.l.
http://dx.doi.org/10.1016/j.ceramint.2013.03.060

effective as a sintering aid for high temperature proton conductor [14–17]. Balibo and Haile showed that ZnO was an excellent sintering aid for yttrium-doped $BaZrO_3$, lowering the densification temperature from 1700 °C to 1300 °C [14]. Tao et al. found that doped $BaCeO_3$–$BaZrO_3$ solid solution with 4 mol% ZnO displayed a good combination of stability, sinterability and conductivity. Wang et al. [18] reported that $BaCe_{0.5}Zr_{0.3}Y_{0.2}O_{2.9}$+$y$ZnO had a densification structure after being sintered at 1300 °C and considered that ZnO was responsible for the sintering densification.

BZY10:BCY10 core–shell structured materials have been investigated [9,10]. However, in their works, because BCY10 was used as shell material, we were still concerned about the chemical stability of the material against CO_2 and H_2O and the densification temperatures for the core–shell materials were also relatively high. In the meanwhile, because the main phase in the BZY10:BCY10 core–shell structured materials was BZY10, their electrical conductivity was also limited.

In this work, we proposed a new core–shell material, in which BCY10 particles as core prepared by the solid reaction were coated by a sol–gel deposited thin shell of BZY10. In order to improve sintering property of the core–shell material, 4 mol% ZnO was added into BZY10 during the sol–gel process. By this work, we expected that BZY10 shell on BCY10 particles could improve the chemical stability, but did not obviously affect the electrical conductivity of BCY10 and 4 mol% ZnO added into BZY10 as a sintering aid could lower densification temperature. The influences of BCY10/BZY10 ratios on the phase purity, microstructure, chemical stability against CO_2 and water vapor and electrical conductivity of the samples were investigated.

2. Experimental

BCY10 was synthesized by the solid state reaction method. Stoichiometric amounts of $BaCO_3$, CeO_2, and Y_2O_3 powders were mixed with ethanol for 24 h in a ball mill using a polyvinylchloride (PVC) jar and ZrO_2 balls. The mixture was dried naturally in air and ground in an agate mortar. Then the dried powders were calcined at 1400 °C in air for 5 h and ground by ball-milling for 48 h to obtain BCY10 powder as core. BZY10 precursor hydrogel was prepared by the sol–gel process. Firstly, stoichiometric amounts of $Ba(NO_3)_2$, $Zr(NO_3)_4 \cdot 5H_2O$, $Y(NO_3)_3 \cdot 6H_2O$ and 4 mol% $Zn(NO_3)_2 \cdot 6H_2O$ were dissolved in distilled water in a beaker; secondly, citric acid as a complexing agent was added into the above solution and homogenized, in which the molar ratio of citric acid to metal ions was 1.5:1. Then BCY10 powder was added to the solution in different weight proportions (BCY10:BZY10=90:10, 80:20, and 70:30); under strong stirring, the ammonia solution was dropped into the solution until the pH value was about 8. After thorough mixing using ultrasound, the final slurry was slowly evaporated at 80 °C to form a viscous gel. The dried gel was then placed in an alumina crucible and calcined at 600 °C in air for 5 h to obtain core–shell structured powders. The powders were pressed into pellets at 25 Mpa and then sintered at 1300 °C in air for 10 h to achieve dense pellets with core–shell structure (BCY10-csh-BZY10).

Phase composition of the materials was characterized by X-ray diffraction (XRD, X'pert Pro) at room temperature using Cu Kα radiation. The XRD patterns were obtained in the 2θ range between 10° and 90° with a step size of 0.02° and a scanning rate of 10°/min. The morphology and the grain size of the powders were examined using transmission electron microscopy (TEM, JEM-2010). During analysis, the samples were hand ground, suspended in ethanol and any agglomerated particles were ultrasonically separated before depositing drops of the suspension. Microstructure of densified pellets was examined by scanning electron microscopy (SEM, S4800).

The chemical stability of samples against CO_2 was determined using a gravimetric method. The powders obtained by grinding sintered pellets were placed in the crucible of a STA449C thermobalance, and 100% CO_2 was then flowed over the powder while the temperature was increased from room temperature to 1300 °C at 10 °C min^{-1}. Weight changes were measured and recorded by the thermobalance.

To test chemical stability of samples to water vapor, humid Ar saturated with water vapor at 80 °C passed over the sample powders at 750 °C for 10 h and then the samples were measured by XRD.

The electrical conductivity of the samples was investigated by AC impedance technique using IM6e electrochemical workstation over the frequency range 0.01 Hz–1 MHz from 300 °C to 800 °C with an interval of 50 °C in air, argon, and humid 4% H_2 (with Ar to balance) at an applied voltage of 5 mV. Before measurement, platinum paste was applied as electrodes onto the surfaces of polished sample pellet and then fired at 900 °C for 0.5 h.

3. Results and discussion

3.1. Phase composition

Fig. 1A shows the XRD patterns of BCY10, 90BCY10-csh-10BZY10 (BCY10:BZY10=90:10), 80BCY10-csh-20BZY10 (BCY10:BZY10=80:20), 70BCY10-csh-30BZY10 (BCY10:BZY10=70:30) and BZY10 after being sintered at 1300 °C. The XRD patterns for BCY10 and BZY10 were in agreement with their standard patterns with the perovskite structure. In fact, BCY was a distorted perovskite oxide with an orthorhombic structure (a=6.243 Å, b=6.209 Å, and c=8.771 Å), while BZY had a cubic cell with crystal lattice parameter of about 4.203 Å [19]. According to Fig. 1, the core–shell structure samples in each composition comprised two distinct phases corresponding to BCY10 and $BaCe_{0.4}Zr_{0.6}O_3$ (Fig. 1B), but BZY10 peaks did not appear. It could be concluded that some migration of cerium into the BZY10 occurred and solid solution $BaCe_{0.4}Zr_{0.6}O_3$ was formed during preparation. This result was not in agreement with the core–shell materials described by Khani et al. [10], where no obvious migration was observed between BYZ10 and BCY10 because their samples were treated at 900 °C. As we saw that the diffraction peaks of BCY10 and $BaCe_{0.4}Zr_{0.6}O_3$ in the XRD patterns were

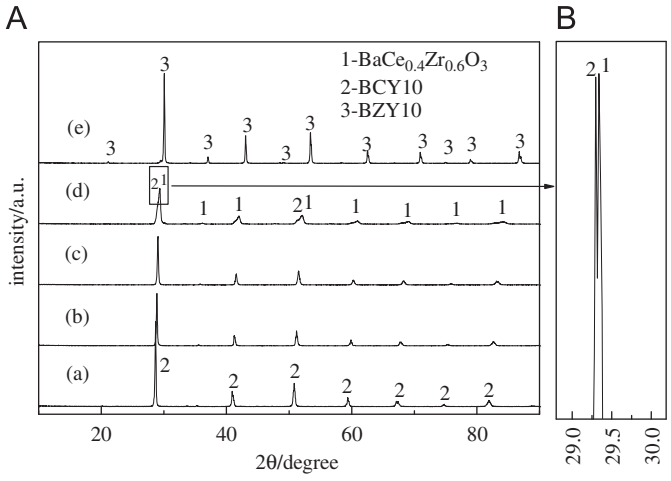

Fig. 1. (A) X-ray diffraction pattern of samples sintered at 1300 °C (a) BCY10, (b) 90BCY10-csh-10BZY10, (c) 80BCY10-csh-20BZY10, (d) 70BCY10-csh-30BZY10 and (e) BZY10; (B) a local magnification of diffraction peaks from A(d).

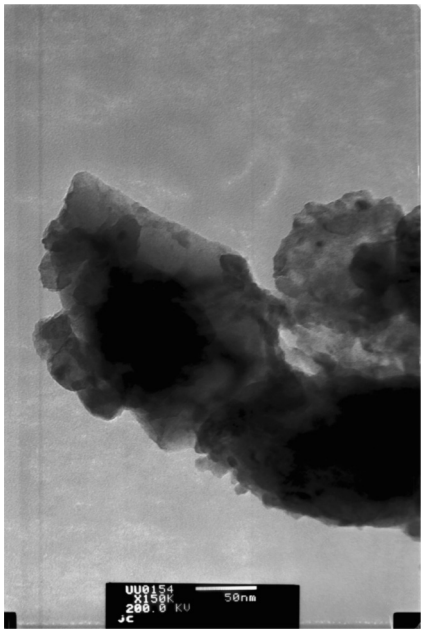

Fig. 2. TEM photographs of 70BCY10-csh-30BZY10 powder sintered at 1300 °C.

too close to each other, it was difficult to distinguish $BaCe_{0.4}Zr_{0.6}O_3$ peaks from BCY10 peaks in the core–shell samples, especially when BZY10 proportion in core–shell samples became small. However, both core BCY10 and shell $BaCe_{0.4}Zr_{0.6}O_3$ phases could be identified after the strongest diffraction peaks were magnified (Fig. 1B).

3.2. Microstructure

Fig. 2 shows TEM photograph of 70BCY10-csh-30BZY10 powder calcined at 1300 °C. The crystallites were nanometric in dimension and the average particle size was about 110 nm. These images showed the BCY10 core (dark area) surrounded by the $BaCe_{0.4}Zr_{0.6}O_3$ shell (light area). Although original composition was BCY10:BZY10 equal to 70:30, because of the formation of $BaCe_{0.4}Zr_{0.6}O_3$ solid solution, the shell volume increased from 30% to about 50%.

Figs. 3 and 4 shows SEM photographs of the surface and cross-section of sample pellets after being sintered at 1300 °C. At this scale, it was not possible to distinguish the core–shell form of the grains. However larger grains surrounded by small ones were observed in the core–shell surface fracture images. BZY10 was notoriously difficult to produce with high density and was quoted as requiring extreme conditions such as sintering at 1700 °C to achieve a density of >95% [20]. In this study, because of application of the sol–gel process in preparation of BZY10 shell and especially the addition of ZnO as sintering aid, a sintering temperature of 1300 °C was sufficient to obtain the dense core–shell samples, as shown in Figs. 3 and 4. The core–shell proportions affected the sample density. With the increase in BZY10 proportion, the sample pellet density decreased. The relative densities of 90BCY10-csh-10BZY10, 80BCY10-csh-20BZY10, and 70BCY10-csh-30BZY10 were 98%, 96% and 95%, respectively. SEM photographs of the cross-section of the samples also verified this result (Fig. 4).

3.3. Chemical stability

The chemical stability in CO_2 atmosphere of the core–shell materials 90BCY10-csh-10BZY10, 80BCY10-csh-20BZY10, and 70BCY10-csh-30BZY10 was examined by the thermogravimetric analysis (TGA) method in 100% CO_2 and the results were compared with that of BCY10. As shown in Fig. 5, a weight increase was observed for all samples. However, BCY10 began to carbonate at temperature over 400 °C (Fig. 5a) and the core–shell materials could resist carbonation until 600 °C (Fig. 5b–d). At 800 °C, the weight gain for all samples reached a maximum value and the weight was kept unchanged until 1050 °C. Above 1050 °C, the carbonation process was reversible, CO_2 began to be eliminated and the process reached completed at 1200 °C. The highest CO_2 uptake was observed to reach 11.1% for the BCY10 powder, which was in agreement with the previous report [10]. For the core–shell materials, the CO_2 uptake significantly lowered, being 3.5%, 2.1% and 1.5% for 90BCY10-csh-10BZY10, 80BCY10-csh-20BZY10, and 70BCY10-csh-30BZY10 respectively. The result implied that the surface of BCY particles was enrobed by a solid solution $BaCe_{0.4}Zr_{0.6}O_3$ which was formed by the reaction between BCY10 and BZY10, reducing the CO_2 uptake. With the increase in BZY10 proportion, thicker $BaCe_{0.4}Zr_{0.6}O_3$ shell was formed, resulting decreased in the CO_2 uptake. As we expected that the chemical stability of BCY10-csh-BZY10 samples against CO_2 was better than that of BZY10-csh-BCY10, because the CO_2 uptake of 10BZY10-csh-90BCY10, 20BZY10-csh-80BCY10, and 30BZY10-csh-70BCY10 was about 5–9% under the same condition [10]. So the BCY10-csh-BZY10 materials were promising for a proton ceramic fuel cell, H_2 permeable membrane and sensors.

The XRD patterns of the core–shell samples after being exposed to flowing water vapor atmosphere at 750 °C for 10 h

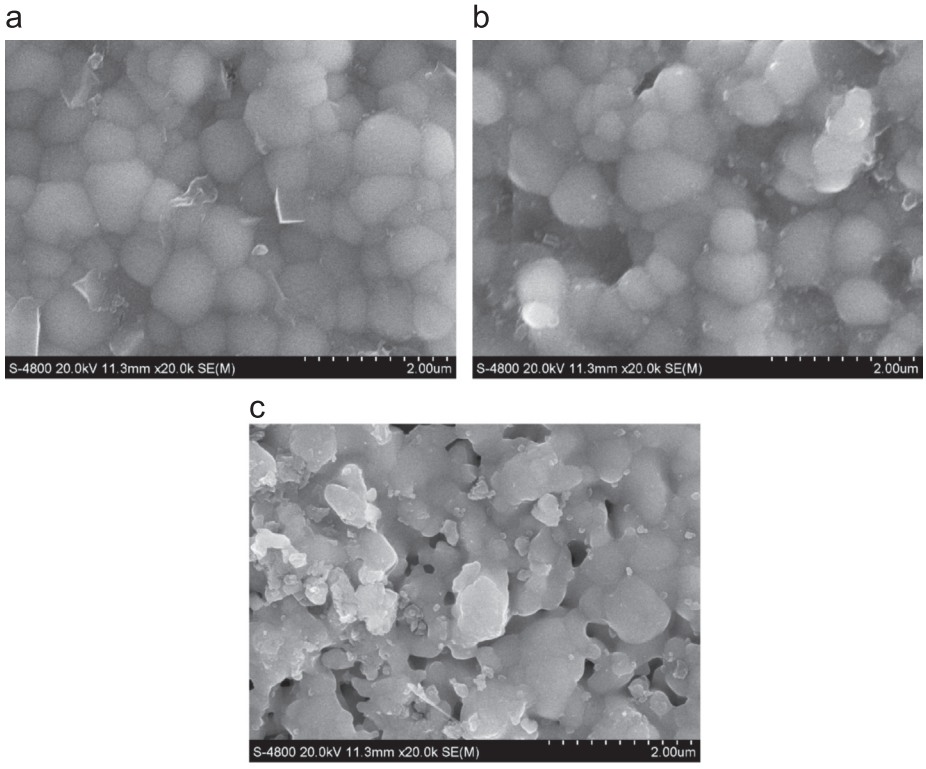

Fig. 3. Surface SEM photographs of sample pellets sintered at 1300 °C: (a) 90BCY10-csh-10BZY10, (b) 80BCY10csh20BZY10 and (c) 70BCY10-csh-30BZY10.

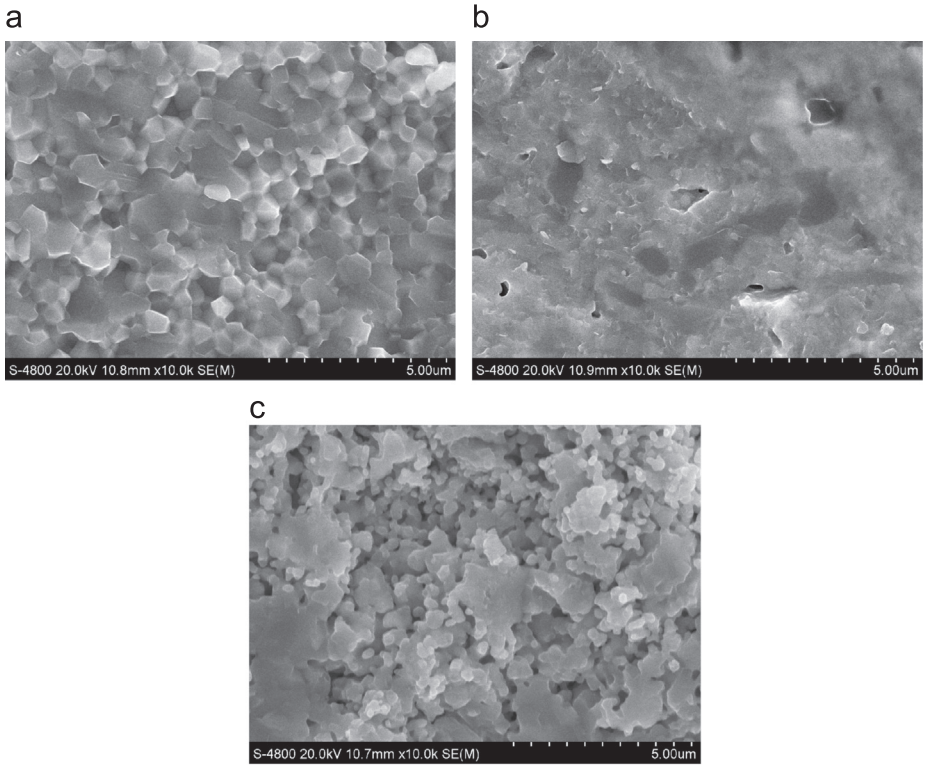

Fig. 4. Cross-section SEM photographs of sample pellets sintered at 1300 °C: (a) 90BCY10-csh-10BZY10, (b) 80BCY10-csh-20BZY10 and (c) 70BCY10-csh-30BZY10.

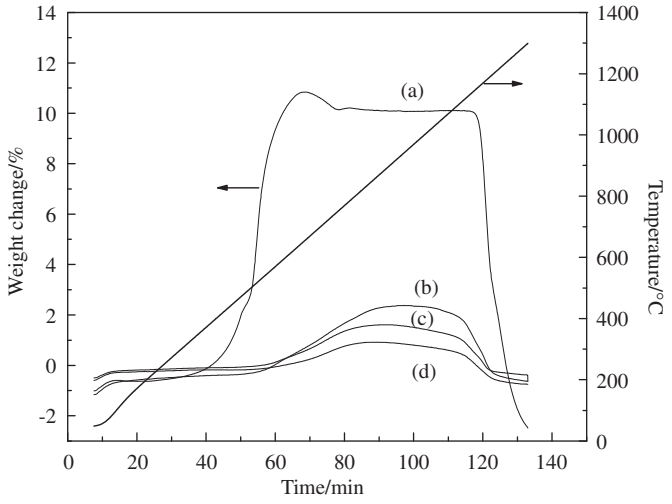

Fig. 5. Thermogravimetric analysis results for sample powders in a CO_2 atmosphere: (a) BCY10 (b) 90BCY10-csh-10BZY10, (c) 80BCY10-csh-20BZY10 and (d) 70BCY10-csh-30BZY10.

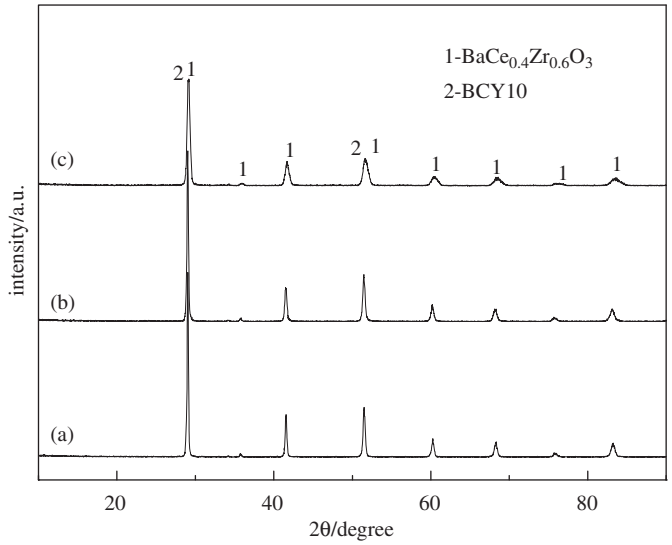

Fig. 6. XRD patterns of samples after being exposed to flowing water vapor atmosphere at 750 °C for 10 h: (a) 90BCY10-csh-10BZY10, (b) 80BCY10-csh-20BZY10 and (c) 70BCY10-csh-30BZY10.

were shown in Fig. 6. The samples kept perovskite structure and all peaks were sharp and no new phase was found, showing that the above core–shell materials were stable against water vapor.

3.4. Electrical conductivity

Fig. 7 shows a set of typical Nyquist plots (Z′ vs. Z″) of 80BCY10-csh-20BZY10 sample recorded in air as well as equivalent circuit models (inset). In the ideal system, the impedance spectra consisted of a set of the semicircles and typical equivalent electrical circuit consisting of parallel resistance–capacitance (*R*–*C*) blocks connected in series was applied to fit the impedance spectra [21]. Bulk and boundary contributions could be identified by typical resistance and capacitance values determined from $2\pi f_{max}RC=1$, where f_{max} was the applied frequency at arc maximum and *R* arc magnitude [22]. In fact, most of the impedance spectra usually showed depressed arcs (such as Fig. 7) and a well established approach was the replacement of *C* by a phenomenological constant-phase element (*CPE*) [21].

The impedance spectrum of 80BCY10-csh-20BZY10 sample at 350 °C showed three arcs: the high-frequency arc corresponded to bulk (grain interior) transport, the intermediate frequency arc represented grain boundary transport and the low frequency corresponded to electrode processes. The alternative equivalent circuit was $L_sR_s(R_bCPE_b)(R_{gb}CPE_{gb})(R_eCPE_e)$, where *L* was an autoinductance element, which was associated to the autoinductive effect introduced by the equipment; R_s was a serial resistance; R_b and CPE_b were the resistance and pesudocapacitance of bulk, R_{gb} and CPE_{gb} were the resistance and pesudocapacitance of grain boundary, R_e and CPE_e were the resistance and pesudocapacitance of the electrode process respectively. With the increase in measurement temperature, the time constants decreased and the arcs shifted to higher frequencies. Therefore, only part of the arcs appeared in the impedance spectra because of the limited frequency range of the equipment. For example, the bulk contribution disappeared at 600 °C. In this case, the equivalent circuit used to fit the spectrum became into $L_sR_s(R_{gb}CPE_{gb})(R_eCPE_e)$. The equivalent circuit for impedance spectrum at 800 °C was the same as that at 600 °C. As shown in Fig. 7, the fitting results based on corresponding equivalent circuit agreed well with the experimental data. The fitting parameters for the impedance spectra at 350, 600 and 800 °C were summarized in Table 1.

The bulk and grain boundary resistances from fitting results were used to obtain the total conductivity for the samples. The total conductivity could be calculated by the equation: $\sigma = \frac{L}{RS}$, where σ, *L*, *S* and *R* represent the total conductivity, the thickness, surface area, and the total resistance of the sample pellets, respectively. The relationship between conductivity and temperature for the samples is plotted in Fig. 8. In the core–shell material series, with increasing BZY10 proportion in the samples, the total conductivity decreased gradually. At 500 °C, the total conductivities are 2.59×10^{-3}, 1.80×10^{-3}, and 9.63×10^{-4} S cm^{-1} for samples containing 10, 20 and 30 wt% BZY10, respectively, which was higher than that reported by Irvine for a solid solution type core–shell material (2.5×10^{-4} S cm^{-1} at 500 °C) [9]. The total conductivity depended not only on the intrinsic conductivity of the components but also on the relative density of the sample, which tended to lower values as the proportion of BZY10 increases. The conductivity values of 90BCY10-csh-10BZY10 sample were higher than those of 90BCY10/10BZY10 solid solution samples with similar proportion prepared by physical mixture [10]. It could be seen from Fig. 8 that the total conductivity of samples followed Arrhenius behavior. According to the Arrhenius equation; $\sigma = \frac{A}{T}\ exp\left(-\frac{Ea}{KT}\right)$ (where *A*, *K*, and *T* are the pre-exponential factor, Boltzmann constant and absolute temperature, respectively), the activation energy for electrical conduction E_a could be determined. E_a for 90BCY10-csh-10BZY10, 80BCY10-csh-20BZY10 and 70BCY10-csh-30BZY10 samples were 0.57, 0.60 and 0.61 eV, respectively. It

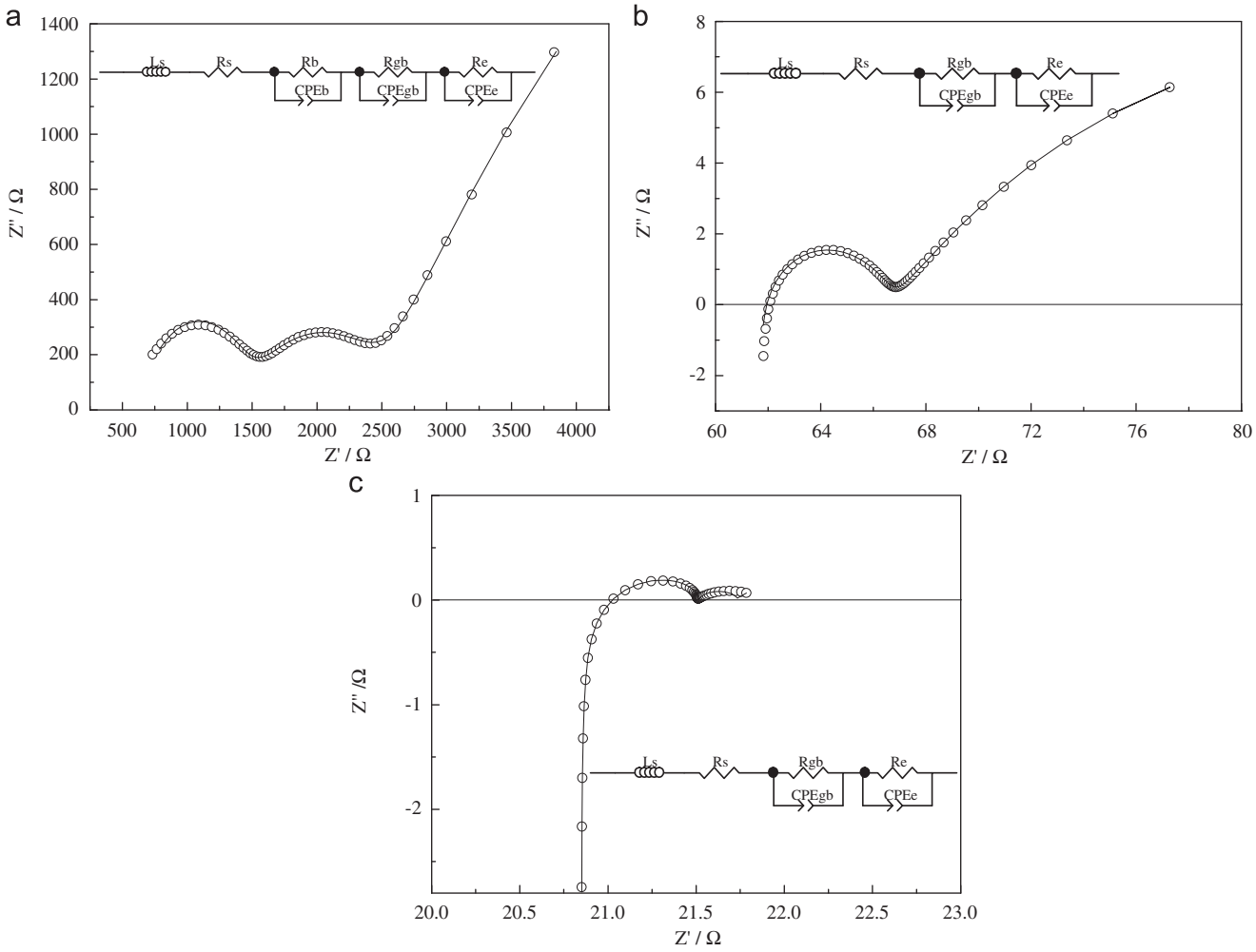

Fig. 7. Typical impedance spectra for 80BCY10-csh-20BZY10 pellet measured at (a) 350 °C, (b) 600 °C, and (c) 800 °C. —: fitting results based on equivalent circuits, ○: experimental data.

Table 1
Fitting parameters for the impedance spectra of 80BCY10-csh-20BZY10 sample at 350, 600 and 800 °C.

	350 °C	600 °C	800 °C
L_s	7.802E−12	2.829E−7	1.393E-6
R_s	551.9	61.63	20.96
CPE_b	1.493E-5		
R_b	876.1		
CPE_{gb}	1.453E-7	4.168E-5	1.371E-5
R_{gb}	988.4	5.032	0.5459
CPE_e	0.0006139	0.05614	1.174
R_e	1.786E4	36.14	0.3213

implied that activation energy became larger with the increasing proportion of the BZY10 shell.

In order to investigate the atmosphere effect on electrical conductivity of the core–shell samples, impedance spectra of 90BCY10-csh-10BZY10 sample were measured in wet 4% H_2/Ar, Ar and air. Fig. 9 shows the relationship between total

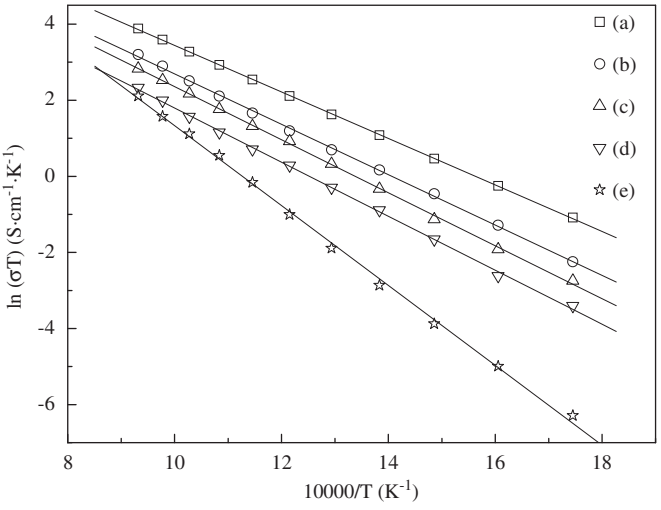

Fig. 8. The relationship between conductivity and temperature of samples measured in air (a) BCY10, (b) 90BCY10-csh-10BZY10, (c) 80BCY10-csh-20BZY10, (d) 70BCY10-csh-30BZY10 and (e) BZY10.

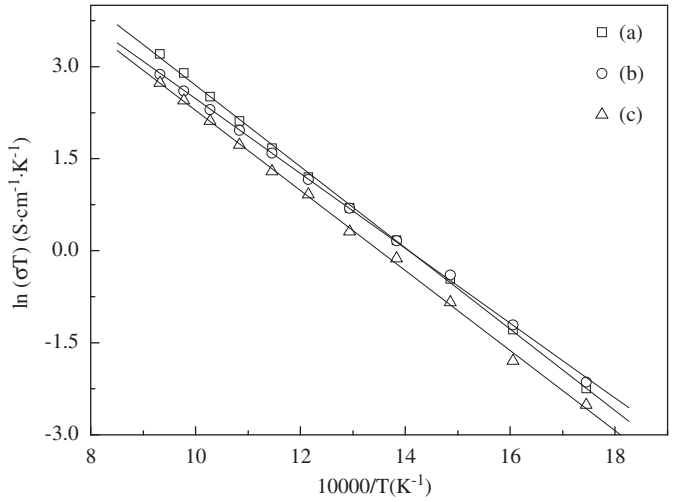

Fig. 9. The relationship between conductivity and temperature of 90BCY10-csh-10BZY10 sample measured in (a) air, (b) wet 4% H_2/Ar, and (c) Ar.

conductivities and temperature at three different atmospheres for 90BCY10-csh-10BZY10 sample. Generally, the conductivity enhanced with the increasing temperature and changed with varying atmospheres. At low temperature, the total conductivity in wet 4% H_2/Ar was higher than that in Ar and air. However, at high temperature the conductivity in air was higher than that in Ar and wet 4% H_2/Ar. Based on Arrhenius equation, the activation energies for 90BCY10-csh-10BZY10 sample in wet 4% H_2/Ar, Ar and air were 0.53, 0.56 and 0.57 eV, respectively. The sample had the lowest activation energy in wet 4% H_2/Ar.

4. Conclusions

(1) BCY10-csh-BZY10 materials were synthesized by sol–gel depositing a thin layer of BZY10 on the surface of BCY10 particles prepared by the solid reaction. The core–shell samples comprised two distinct phases corresponding to BCY10 and $BaCe_{0.4}Zr_{0.6}O_3$. The average particle size was about 110 nm and BCY10 core was wrapped by a thin layer of $BaCe_{0.4}Zr_{0.6}O_3$ shell. The samples had a high density after being sintered at 1300 °C, because of addition of ZnO sintering aid.

(2) BCY10-csh-BZY10 samples displayed improved stability against CO_2 by the TGA. With BCY10-csh-BZY10 proportions varying from 9:1 to 7:3, the samples became more stable. All the core–shell samples also were relatively stable in water vapor under tested conditions.

(3) The conductivities of BCY10-csh-BZY10 decreased with core–shell ratio varying from 9:1 to 7:3; the conductivity value of 90BCY10-csh-10BZY10 sample was higher than that of BCY10/BZY10 solid solution samples with similar composition prepared by physical mixture.

Acknowledgments

The authors acknowledge the financial support from the National Natural Science Foundation of China under Grant nos. 50972038 and 51272067, and the Iron–Steel United Foundation of Hebei Province under Grant nos. E2011209036 and E 2012209018.

References

[1] H. Iwahara, T. Esaka, H. Uchida, N. Maeda, Proton conduction in sintered oxides and its application to steam electrolysis for hydrogen production, Solid State Ionics 3–4 (1981) 359–363.
[2] H. Matsumoto, H. Hayashi, T. Shimura, K. Amezawa, T. Otake, K. Yashiro, Y. Nigara, A. Kaimai, T. Kawada, H. Iwahara, J. Mizusaki, Hydrogen isotope sensor using high temperature proton conductors, Solid State Ionics 175 (2004) 491–495.
[3] M. Tanaka, K. Katahira, Y. Asakura, T. Ohshima, Hydrogen pump using a high-temperature proton conductor for nuclear fusion engineering applications, Solid State Ionics 181 (2010) 215–218.
[4] Z. Tao, Z. Zhu, H. Wang, W. Liu, A stable $BaCeO_3$-based proton conductor for intermediate-temperature solid oxide fuel cells, Journal of Power Sources 195 (2010) 3481–3484.
[5] M. Ni, M.K.H. Leung, D.Y.C. Leung, Technological development of hydrogen production by solid oxide electrolyzer cell (SOEC), International Journal of Hydrogen Energy 33 (2008) 2337–2354.
[6] K.D. Kreuer, Proton-conducting oxides, Annual Review of Materials Research 33 (2003) 333–359.
[7] K.H. Ryu, S.M. Haile, Chemical stability and proton conductivity of doped $BaCeO_3$–$BaZrO_3$ solid solutions, Solid State Ionics 125 (1999) 355–367.
[8] S.M. Haile, G. Staneff, K.H. Ryu, Non-stoichiometry, grain boundary transport and chemical stability of proton conducting perovskites, Journal of Materials Science 36 (2001) 1149–1160.
[9] C.D. Savaniu, J.C. Vazquez, J.T.S. Irvine, Investigation of proton conducting $BaZr_{0.9}Y_{0.1}O_{2.95}$: $BaCe_{0.9}Y_{0.1}O_{2.95}$ core–shell structures, Journal of Materials Chemistry 15 (2005) 598–604.
[10] Z. Khani, M.T. Jacquin, G. Taillades, D.J. Jones, M. Marrony, J. Rozière, Preparation of nanoparticle core–shell electrolyte materials for proton ceramic fuel cells, Chemistry of Materials 22 (2010) 1119–1125.
[11] I. Haq, E. Matijević, Preparation and properties of uniform coated inorganic colloidal particles, Journal of Colloid and Interface Science 192 (1997) 104–113.
[12] C.J. Brinker, G.W. Scherer, Sol–Gel Science: The Physics and Chemistry of Sol–Gel Processing, Academic Press, New York63–77.
[13] G.R. Lee, J.A. Crayston, Sol–gel processing of transition-metal alkoxides for electronics, Advanced Materials 5 (1993) 434–442.
[14] P. Babilo, S.M. Haile, Enhanced sintering of yttrium–doped barium zirconate by addition of ZnO, Journal of the American Ceramic Society 88 (2005) 2362–2368.
[15] J.S. Park, J.H. Lee, H.W. Lee, B.K. Kim, Low temperature sintering of $BaZrO_3$-based proton conductors for intermediate temperature solid oxide fuel cells, Solid State Ionics 181 (2010) 163–167.
[16] C. Zhang, H. Zhao, N. Xu, X. Li, N. Chen, Influence of ZnO addition on the properties of high temperature proton conductor $Ba_{1.03}Ce_{0.5}Zr_{0.4}Y_{0.1}O_{3-\delta}$ synthesized via citrate–nitrate method, International Journal of Hydrogen Energy 34 (2009) 2739–2746.
[17] I. Karaca, O. Uzun, U. Kölemen, F. Yılmaz, O. Sahin, Effects of ZnO addition on mechanical properties of $Bi_{1.84}Pb_{0.34}Sr_{1.91}Ca_{2.03}Cu_{3.06}O_{10}$ prepared by a wet technique, Journal of Alloys and Compounds 476 (2009) 486–491.
[18] H. Wang, R. Peng, X. Wu, J. Hu, C. Xia, Sintering behavior and conductivity study of yttrium-doped $BaCeO_3$–$BaZrO_3$ solid solutions using ZnO additives, Journal of the American Ceramic Society 92 (2009) 2623–2629.
[19] E. Fabbri, D. Pergolesi, A. D'Epifanio, E.D. Bartolomeo, G. Balestrino, S. Licoccia, E. Traversa, Design and fabrication of a chemically-stable proton conductor bilayer electrolyte for intermediate temperature solid oxide fuel cells (IT-SOFCs), Energy and Environmental Science 1 (2008) 355–359.

[20] P.A. Stuart, T. Unno, R. Ayres-Rocha, E.l. Djurado, S.J. Skinner, The synthesis and sintering behaviour of $BaZr_{0.9}Y_{0.1}O_{3-\delta}$ powders prepared by spray pyrolysis, Journal of the European Ceramic Society 29 (2009) 697–702.

[21] Y.M. Guo, R. Ran, Z.P. Shao, S.M. Liu, Effect of Ba nonstoichiometry on the phase structure, sintering, electrical conductivity and phase stability of $Ba_{1\pm x}Ce_{0.4}Zr_{0.4}Y_{0.2}O_{3-\delta}$ ($0\leq x\leq 0.20$) proton conductors,, International Journal of Hydrogen Energy 36 (2011) 8450–8460.

[22] Y.F. Zheng, S.C. He, L. Ge, M. Zhou, H. Chen, L.C Guo, Effect of Sr on Sm–doped ceria electrolyte, International Journal of Hydrogen Energy 36 (2011) 5128–5135.